Proton Transport Property in Supported Nafion Nanothin Films by Electrochemical Impedance Spectroscopy

Devproshad K. Paul,[a,b] Richard McCreery,[c,*] and Kunal Karan[b,,z]**

[a]*Department of Chemical Engineering, Queen's University, Kingston, ON K7L 3N6, Canada*
[b]*Department of Chemical and Petroleum Engineering, University of Calgary, Calgary, AB T2N 1N4, Canada*
[c]*Department of Chemistry, University of Alberta, Alberta, Canada*

The proton transport property of Nafion nanothin films (4–300 nm) has been investigated by electrochemical impedance spectroscopy (EIS) using interdigitated array (IDA) of gold electrodes on SiO_2 substrate. The proton conductivity has been investigated as a function of film drying/heating protocol, relative humidity, temperature and film thickness. It is found that the film treatment protocol makes a difference in film transport property. Ultimately, the proton conductivity and capacitance of the Nafion nanothin film is thickness-dependent, where the former decreased and the latter increased exponentially with decreasing film thickness. Moreover, the activation energy increased exponentially with decreasing film thickness. The proton conductivity of the thin films of Nafion is significantly lower than that of the membrane counterpart regardless of the thickness, which is consistent with the high activation energy found in the thin films. These differences are likely related to the polymer confinement and morphological differences between the thin films and the freestanding membrane.
 [DOI: 10.1149/2.0571414jes] All rights reserved.

Manuscript submitted August 19, 2014; revised manuscript received September 30, 2014. Published October 8, 2014.

Proton transport is a key functional property of the ionomer used in polymer electrolyte based energy conversion and storage devices including polymer fuel cells (PEFC),[1] polymer electrolyte membrane (PEM) water electrolyzers,[2] photo electrochemical cells[3,4] and artificial photosynthesis device.[5] For PEFCs and PEM electrolyzers, Nafion is the most extensively employed. As a freestanding film of thickness (25–100 μm thick), Nafion serves the function of the electrolyte membrane separating the anode and the cathode. The ionomer is also present in the electrochemically active component of these energy conversion devices as a thin film coating the electrocatalyst. For example, the conventional PEFC catalyst layer (CL) is a porous composite layer (10–25 μm thick) of Platinized carbon (Pt/C) and ionomer. In the CL, the ionomer forms a semi-continuous, web-like nanothin film (4–10 nm) covering the aggregates of Pt/C.[1,6] The thickness of such nanothin Nafion films in the CL is comparable to the ionic domain size (∼4 nm) in the bulk Nafion membrane.[7,8] It is obvious that the ionomer structure and property will affect both the proton and mass transport, which in turn will impact the local electrochemical reaction rate and, thereby, the overall PEFC performance. In fact, researchers of the electrochemical energy research laboratory at General Motors (GM)[9] examined the electrode performance as a function of catalyst loading and found that low-Pt loading catalyst layers exhibited higher transport losses, which they attributed to the transport resistance of ionomer thin film covering the catalyst. The proton conductivity of Nafion membrane is widely investigated and discussed in the literature.[10–13] In contrast, the proton conductivity of thin Nafion film has remained relatively unexplored, especially for ionomer films of thickness comparable to ionic domain size (∼4–5 nm). The ionic conduction property of materials is highly regulated by its nano-structural or morphological features such as ionic domain shape and size and the inter-connectivity of the domains. Recent studies have indicated that the nanostructure and morphology of thin Nafion films are different from those of thicker Nafion membrane.[14–23] One of the main reasons is the high interfacial area to volume ratio of thin films such that the substrate induced interfacial and confinement effect dominate the film morphology and properties.[24] This raises a few questions – (i) is the proton conductivity and conduction mechanism of supported thin films different than that of the freestanding membrane? (ii) if so, what factors are responsible for the possible differences in proton transport?

To the best of our knowledge, in addition to our data on 50 nm Nafion film,[20] only Siroma et al.[21] have reported proton conductivity of thin Nafion films. Their work showed the Nafion conductivity to be film thickness dependent and the conduction to be associated with higher activation energy. However, they prepared the films by spin coating rather by self-assembly and the lowest thickness for which data was reported was 14 nm. The continuity and homogeneity of such a thin film prepared by spin coating technique is always a concern. Moreover, we have recently shown that there are differences between spin-coated and self-assembled films in morphology and water activity.[25] Nagao et al.[26] studied spin coated Nafion thin films on silica substrate using Infrared p-polarized multiple-angle incidence resolution spectrometry (IR p-MAIRS) technique and made inferences about low proton conductivity in such films. They indicated that highly oriented sulfonic acid group in the substrate/film interface might be related to the low proton conductivity. However, they investigated comparatively thicker film (∼150 nm).

Activation energy of proton conduction can be considered as a useful parameter that may provide insight into the dominant transport mechanism. The activation energy of Nafion 117 equilibrated with liquid water has been reported to vary from 9 to 14 kJ/mol[27,28] while those for Nafion 120[11] and Nafion 112[21] are close to 15 kJ/mol. The three different bulk Nafion membrane (Nafion-112, 117, and 120) differing in thickness exhibit similar activation energy indicating similar intrinsic properties of the bulk membrane including molecular orientation and arrangement behavior. The proton transport mechanism in Nafion membrane has been described as a combination of surface diffusion, Grotthuss (hopping) and vehicular/en-mass diffusion.[29–34] Each mechanism has a characteristic activation energy and the dominant transport mechanism is known to vary with Nafion water content, which depends both on the local environmental conditions (temperature and relative humidity) and polymer nanostructure. Therefore, the variation either in the nano-structure/orientation or in the transport mechanism may change the activation energy.

The characteristics of the self-assembled Nafion thin films were described in our recent publications[35,36] but the focus of those studies was thickness-dependent surface morphologies and wettability. Two distinct surface characteristics were noted; films of thickness 55 nm and less exhibited hydrophilic surface whereas films greater than 55 nm in thickness were hydrophobic. A nanostructure for the films was proposed wherein the substrate-induced organization of Nafion in lamellar form extends to ∼55 nanometers. Beyond this thickness of 55 nm, free reorganization of Nafion occurs. Another study[22] also indicated the distinct characteristics of the spin coated Nafion thin films where they found that the swelling ratio, volumetric

*Electrochemical Society Fellow.
**Electrochemical Society Active Member.
zE-mail: kkaran@ucalgary.ca

water fraction, and effective diffusivity of films are relatively constant for spin-coated films thicker than ca. 60 nm but gradually decreased with decreasing thickness. It has been proposed that there may be a substrate induced re-orientation[14–17] and thickness-dependent gradual change in organization[35] of the Nafion bundles resulting in a change of morphology.[37] Transport characteristics of the self-assembled films may be a reflection of the morphological and structure features.

In this paper, the proton transport behavior of self-assembled Nafion nanothin films varying in thickness from 4 nm to 300 nm is presented. Electrochemical Impedance Spectroscopy (EIS) was employed for impedance measurement of the Nafion nanothin films on inter-digitated array (IDA) of gold (Au) electrode supported by SiO_2/Si wafer. Film conductivity as a function of relative humidity and temperature was determined for films of various thicknesses. The films were subjected to different post-fabrication treatments and the effect of the treatment was investigated. A comparison of the conductivity and activation energy of the nanothin films with those of its membrane counterpart is reported.

Experimental

Materials.— Commercially available 5 wt% Nafion dispersion was used as stock solution for thin film preparation. The self-assembled thin film preparation protocol has been described in detail elsewhere.[35] Isopropyl alcohol (IPA) diluted Nafion dispersion was used for film preparation but SiO_2 supported inter-digitated Au was used. The details of electrode have been included in the supporting information (SI), Figure S1.

Preparation of self-assembled nanothin films on IDA.—Electrode cleaning.— The electrode was soaked into acetone for 30 min followed by sonication for 2 min in each solvent (IPA, acetone and Millipore water). Finally, it was washed repeatedly at least 3 times with a number of solvents including IPA, acetone and Millipore water. The electrode was dried under gentle flow of N_2 stream prior to deposition of ultrathin film on it. Unlike method reported in our prior work,[35] the wafer with gold IDA was not exposed to piranha solution. Highly oxidizing piranha solution can oxidize the underlayers and the metal electrode resulting in a detachment of the electrodes from the SiO_2 surface rather cleaning of the SiO_2 surface. Nonetheless, the impedance of blank electrode was measured before and after cleaning to ensure that the electrode was not damaged during the cleaning steps.

Fabrication of self-assembled Nafion nanothin films on IDA.—The method for generating ionomer film on SiO_2 supported IDA is same as that reported for ionomer films creation on blank SiO_2 substrate.[35] Briefly, 5 wt% Nafion stock dispersion was diluted to 0.1, 0.25, 0.5, 1.0, and 3.0 wt% by adding IPA. The diluted dispersion was equilibrated for 24 h at room temperature. Then, the pre-cleaned electrodes were immersed into the diluted dispersions. From previous work, we found that 12 h is sufficient time to make a homogenous and continuous film on the SiO_2 substrate[35] Accordingly, the substrates were taken out from the Nafion dispersion after immersion for 12 h and dried in N_2 flow. Before impedance measurement, the films subjected to one of the two protocols discussed below. The characteristic film thicknesses – 4 nm, 10 nm, 30 nm, 55 nm, 160 nm and 300 nm were adopted for the 0.1, 0.25, 0.5, 1.0, 3.0 and 5 wt% Nafion dispersion, respectively as reported in our recent publication.[35] Further, the thickness of the films on IDA was also confirmed by AFM scratching method and XPS.

Treatment of self-assembled nanothin films.— The IDA coated with Nafion nanothin film was placed in an environmental chamber (Model 3911, Thermo Forma, USA), equipped with relative humidity (RH) and temperature control, for the further treatment before impedance measurement. The environmental chamber can control temperature from 0 to 60°C and RH ranging from ∼0 to 96%. To maintain RH below the ambient level – especially, close to zero RH, a separate dry air flow was supplied to the chamber. Since water uptake and morphological changes of the film can significantly influence the proton conductivity, two treatments protocols (Protocol-1 and Protocol-2), were strictly maintained to get the films equilibrated at a certain temperature and relative humidity. The main point was to avoid any uncertainty of morphological changes at high temperature treatment. On the other hand, the films should be equilibrated at the highest measurement temperature to avoid any over/under-estimation of impedance for temperature dependent measurement.

For both protocol-1 and protocol-2, the initial step was the same – the films were kept in the environmental chamber at ∼25°C and low (almost zero) relative humidity with continuous dry air flow for overnight (15 to 20 h). Protocol -1 was adopted for the impedance measurement at room temperature (25°C), therefore, the impedance data was collected after the initial step and further equilibrating at each RH, ranging from 20 to 95% RH.

Protocol -2 was adopted for measurements at higher than room temperatures (30 to 60°C). The as-prepared film was brought to 60°C and equilibrated at low RH condition. The equilibration was also monitored and confirmed by a single-frequency impedance measurement. Once the equilibration was confirmed, the impedance data of the thin films were collected at 60°C for RH varying from 20% to 96%. In each case, the equilibration was monitored and confirmed. The equilibration monitoring protocol has been described below.

Impedance measurement of the self-assembled nanothin films—Impedance measurement set up.— The measurements were accomplished by a two micro-probe setup connected to a Solartron 1260 frequency-response analyzer coupled to a Solartron 1296 dielectric interface. A humidity sensor (CMOSENS Tec., Switzerland) was placed in the close vicinity of the IDA sample to monitor the local equilibration for RH and temperature. Two other sensors were in the different place of the chamber to monitor the overall equilibration of the chamber termed as external equilibration (See Figure S2 in SI). Although the external RH and temperature equilibrations were rapid and could be monitored by appropriate sensors, it does not guarantee the internal equilibration of film.

Equilibration monitoring protocol.—The equilibration protocol is the combination of external and internal equilibration of the thin film. As observed, the external equilibration established rapidly, which is monitored by the external sensors placed in the environmental chamber. In contrast, internal equilibration - essentially water absorption and polymer relaxation, is a slow process. Since proton conduction is water-mediated, any change in water content of the ionomer directly impacts the ionomer film conductivity. Therefore, a single-frequency impedance measurement was carried out to monitor the approach to ionomer film equilibration. When the impedance value became invariant with time, the film was deemed to be equilibrated at the set RH and temperature. Both external and internal equilibrations were maintained for data collection.

Impedance data collection.—Once the film had internally equilibrated which usually takes 0.5 h to 2 h depending on the humidity and temperature conditions, the impedance data were collected by applying an alternating potential of amplitude 100 mV over a frequency ranging from 10 MHz to 0.01 Hz. At least three repeat measurements were recorded at the same measurement setup to verify reproducibility of the measurements. Smart impedance measurement software (Solartron Analytical) was used for data collection. Z-view impedance software (Version 3.0a, Scribner Associates Inc.) was adopted for equivalent-circuit design, model fitting and data analyses as described in the results and discussions.

Results and Discussion

Impedance responses of Nafion nanothin films.— The typical impedance response of our thin films is comprised of an inductive part, a suppressed semicircle at the high-frequency region and also a vertical-line like response in the low frequency region (Figure 2).

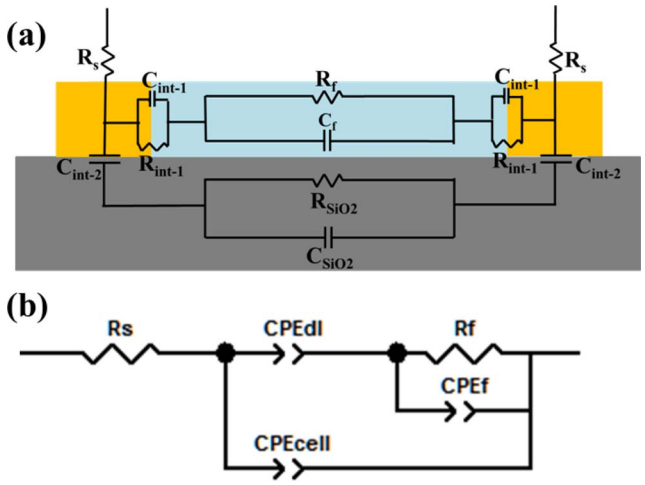

Figure 1. Equivalent circuit model – (a) possible impedance and capacitance components in the Nafion nanofilm on SiO_2 supported IDA gold electrode. Gray color, yellow color and blue colors represent SiO_2, Au and Nafion nanofilm, respectively, (b) simplified equivalent circuit.

Similar response has been reported by others.[10–13] Typically, a slightly depressed semicircle-type response typical of a parallel RC circuit is observed at higher frequency. At the same time, the vertical line represents capacitive behavior only. Impedance responses of thin films for changes in relative humidity, temperature, film thickness and chemical atmosphere has been included in the supporting information (Figure S3 to S6).

The main goal of the impedance measurements is to extract the proton transport resistance attributed by the Nafion thin film. Eventually, the extracted resistance is employed for the calculation of the proton conductivity considering the IDA electrode geometry. Unfortunately, the impedance response does not directly provide film resistance and capacitance unless it is fitted with an appropriate equivalent circuit.

Equivalent circuit design.— To design an appropriate equivalent circuit, it is important to identify the key physical processes of the electrode/film system and represent the processes with a suitable electrical circuit element. An idealized circuit model has been proposed considering all key contributions from the thin film, the cell and the cell connectors in the Figure 1a. Each interface between thin film and electrode has been represented by a parallel combination of capacitance ($C_{int\text{-}1}$) - corresponds to the double layer capacitance, and an interfacial resistance ($R_{int\text{-}1}$). Primarily, it is assumed that Nafion thin film has a film resistance (R_f) in parallel to a film capacitance (C_f). The cell contribution is the combination of the capacitance of electrode/SiO_2 interface ($C_{int\text{-}2}$) and a parallel connection of SiO_2 resistance (R_{SiO2}) and SiO_2 capacitance (C_{SiO2}). Beside the film and cell resistance, there is a serial resistance (R_s) - originating partly from the contact between electrode and probe and partly from the wire resistance, and an inductance (not included in the equivalent circuit) – originating from the long wire connection.

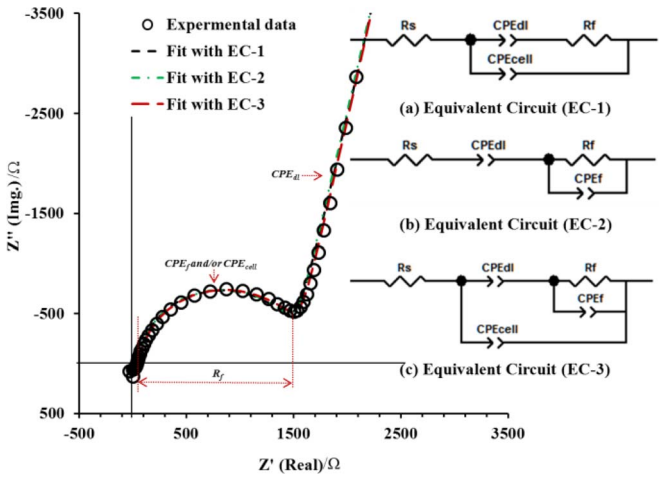

Figure 2. Typical impedance plot of Nafion nanofilm and the fitting with three different equivalent circuits - (a) EC-1 (b) EC-2 and (c) EC-3 (inset).

A simplification of the equivalent circuit with the adequate representation of the real system can be made. For the system under test, the electrode/film interfacial resistance can be omitted since negligible, if any, effect of interfacial reaction was observed at higher frequency. Considering little to no faradaic charge cross the interface, the interfacial response should be solely capacitive – defined as a double layer capacitance. The impedance measurement of blank electrode also shows that the response is highly capacitive at least in the frequency range of 10 MHz to 0.01 Hz. A significantly high resistance for SiO_2 substrate is expected. Therefore, R_{SiO2} was omitted and the electrode/SiO_2 interfacial and SiO_2 capacitance was combined and represented as cell capacitance.

An ideal capacitor response would manifest as a vertical line in the Nyquist plot – Z′ (real) vs Z″ (img.). Moreover, when the ideal capacitance is involved in the parallel combination with the resistance, a semicircle response with definite radius arises. However, a close observation of the typical impedance response reveals that the semicircle was suppressed and the lower frequency response deviates from the ideal (the vertical line) response. One of the reasons for such response is that the capacitance of solid electrolyte deviates from the ideal behavior due the inhomogeneity or surface roughness of the two parallel plates of the capacitor. Therefore, the capacitance is better described by a constant phase element (CPE) according to the expression below:

$$CPE = \frac{1}{(j\omega C)^n} \qquad [1]$$

where, ω ($= 2\pi f$) is the angular frequency and n is the exponent which value varies from 0 to 1. *CPE* depends on both ω and $0 < n < 1$ and *CPE* turns into a pure capacitor when n equals one. The frequency-dependent *CPE* comprises of two elements: *CPE-T* is pseudo capacitance, corresponding to real capacitance *C* and *CPE-P* is related to the roughness of the interphases represented by n in Eq. 1.[10] Based on the above observation and discussion, the capacitance contribution of the cell, film and double layer have been replaced in the simplified equivalent circuit by constant phase elements – CPE_{cell}, CPE_f and CPE_{dl}, respectively. However, the origin and existence of CPE_{cell}, and CPE_f in the impedance response of such systems are still under debate.[5,7,25,26] Soboleva et al.[10] and Yadav et al.[13] have indicated that Nafion membrane has a capacitance in parallel to the resistance. The origin of capacitance has been described as the polarization of water inside the nanopore and the close proximity of the sulfonate group. In contrast, Mikhailenko et al.[38] and Lee et al.[39] found that the capacitance associated with the arc-like response is due to the cell capacitance. Therefore, it is important to understand whether both capacitances significantly contribute or only one of the capacitances dominates in the high-frequency arc of the impedance response. In this study, part of the interest is to investigate the capacitance behavior of the Nafion nanothin films.

To probe the aforementioned issues, three equivalent circuits (ECs) were built: (i) EC-1, [R-CPE_{cell}] (ii) EC-2, [R-CPE_f] and (iii) EC-3, [R-CPE_f-CPE_{cell}]. The equivalent circuits were fitted with the typical impedance response and the values of the pertinent circuit elements have been summarized in Table I. Interestingly, it was found that all of the three ECs could adequately fit the data. The fitting results of the EC-1 and EC-2 were comparable. *CPE* parameters very close in value to each other were obtained though it was attributed to the cell and film contribution of EC-1 and the EC-2, respectively. In contrast, the film resistance obtained from fit of data by EC-1 was 5% higher than that obtained by EC-2. When data was fitted with

Table I. Summarized equivalent circuit fitting parameters with three equivalent circuit considerations.

Equivalent circuit (EC)	EC-1 (only CPE_{cell})	EC-2 (only CPE_f)	EC-3 (both CPE_f and CPE_{cell})
R_s	57.76 Ω	57.10 Ω	60.17 Ω
R_f	1500 Ω	1410 Ω	1411 Ω
CPE-$T_{dl} \approx C_{dl}$	2.58×10^{-07} F	2.60×10^{-07} F	2.54×10^{-07} F
CPE-$P_{dl} \approx n_{dl}$	0.87	0.87	0.87
CPE-$T_f \approx C_f$	–	2.65×10^{-09} F	2.78×10^{-09} F
CPE-$P_f \approx n_f$	–	0.97	0.97
CPE-$T_{cell} \approx C_{cell}$	2.43×10^{-09} F	–	6.3×10^{-19} F
CPE-$P_{cell} \approx n_{cell}$	0.98	–	2.33

EC-3, it was found that the CPE_{cell} was negligibly small whereas the CEP_{cell} and R_f are comparable to that of the EC-2. This would indicate that the simplified equivalent circuit EC-2 may better represent to the real system. However, more investigation is needed to claim the capacitance solely as the film capacitance. It is noted that regardless of ECs discussed above, the fitting parameters are comparable.

Model fitting results provide an insight into the contribution of each element of the equivalent circuit to the impedance response. However, it should be validated based on experimental evidence. In the high-frequency region, the positive values of imaginary impedance, attributed to the inductance of the setup, can be noted. The x-intercept is due to the contact/series resistance R_s. The inductance and R_s contributions were confirmed by the impedance measurement of the shorted cell and the inductive and resistive responses were found to the same as that obtained from the impedance from the cell with Nafion thin film. The diameter of high-frequency arc represents the film resistance, which has been confirmed by the change of arc diameter with changes with three parameters - RH, temperature and thickness of the films (see Figure S3 to S5 in SI). It is noted that the resistance associated in the ionomer is dependent on RH, temperature and thickness. However, electrode reactions are expected to occur during ac impedance measurements since proton conduction in the film must be accompanied with the measured external electronic current. The key question is whether the high-frequency response contains any significant contribution from the interfacial or charge-transfer reaction, for example, those arising from oxygen reduction reaction due to exposure of the electrode to air. Impedance measurements in the absence of oxygen were carried out to investigate if electrode reactions contributed significantly to the high-frequency semi-circle response. It was found that oxygen-free atmosphere produced similar impedance response, which indicates that no significant contribution from the expected oxygen-related charge-transfer reaction exists (the measurement protocol and responses have been included in SI, Figure S6). The associated capacitance has been considered as the film capacitance; this is discussed further in the following. The low-frequency response is capacitive and attributed to the double layer capacitance. The appearance of the double layer capacitance in the low-frequency region of the impedance response has been discussed by others.[10–13,39]

Proton conductivity of the Nafion nanothin films.— The film conductivity (k_f) was calculated from the resistance (R_f) using equation 2, where, d is the spacing between the IDA electrode teeth (100 μm), t is the thickness of the ionomer film, l is the length of the teeth (0.8 cm) and N is the number of electrodes (110). Measurements with different IDA electrode spacings of 30 μm and 500 μm were also carried out and it was found that the proton conductivity calculated from different electrode spacing remained within error (10%) of sample-to-sample measurement (see Figure S11 in SI).

$$k_f = \frac{1}{R_f} \cdot \frac{d}{l(N-1)t} \qquad [2]$$

The proton conductivity of the thin films was measured as a function of two variables, film thickness and relative humidity, at two different temperatures. A comparison of the proton conductivities under two different film treatment protocols is made to investigate whether the treatment protocol becomes a determining factor for the resulted proton conductivity of Nafion thin films.

Proton conductivity at room temperature (25°C).—Proton conductivities of the Nafion thin films with thickness ranging from 4 nm to 300 nm have been presented as a function of relative humidity at 25°C in the Figure 3. The proton conductivity of Nafion 117[12] at 100% RH has also been plotted in the Figure 3 for the comparison between the thin film and the membrane conductivities. As expected, proton conductivity of the thin films increased with increasing relative humidity. Regardless of the thickness, the logarithm of the thin film proton conductivity appears to be a linear function of the relative humidity over two different ranges of humidity. The slope in the 20–40% RH range was higher than that in the 40–95% RH range. The proton conductivity increased rapidly from dry condition to 40% RH but at a much slower rate at a higher RH. Similar behavior of proton conduction with RH has also been observed for the Nafion membrane.[27,43]

It is interesting to note that the proton conductivities of ultra-thin films (4 to 55 nm films) are very comparable to each other. In contrast, the conductivity of thicker films (160 nm and 300 nm films) varies with thickness such that the 300 nm film had conductivity closer to that of Nafion membrane.[10–13] Therefore, the proton conductivity of the ultrathin films is significantly lower than that of the thicker films as well as that of the Nafion membrane. The differences in proton conductivity are more significant at lower RH. At low RH, there was a non-significant dependency of the proton conductivity on thickness up to 55 nm whereas it was about two orders of magnitude higher in thicker films. At high RH, similar lack of dependence of proton conductivity on thickness for films up to 55 nm was observed. However, the difference in the proton conductivity of the ultrathin films (<55 nm) and the thicker films at high RH is 2.5 times compared to a difference of nearly 2 orders of magnitude at low RH.

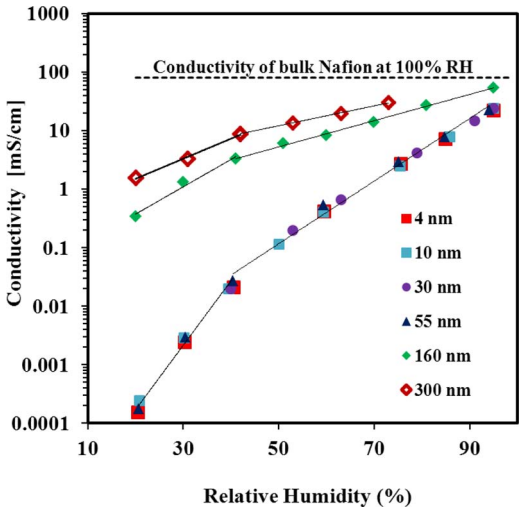

Figure 3. Proton conductivity of the Nafion nanothin films, of various thickness ranging 4 nm to 300 nm, at 25°C as a function of RH; proton conductivity of bulk Nafion 117 membrane[12] (dotted line) at 25°C and 100% RH.

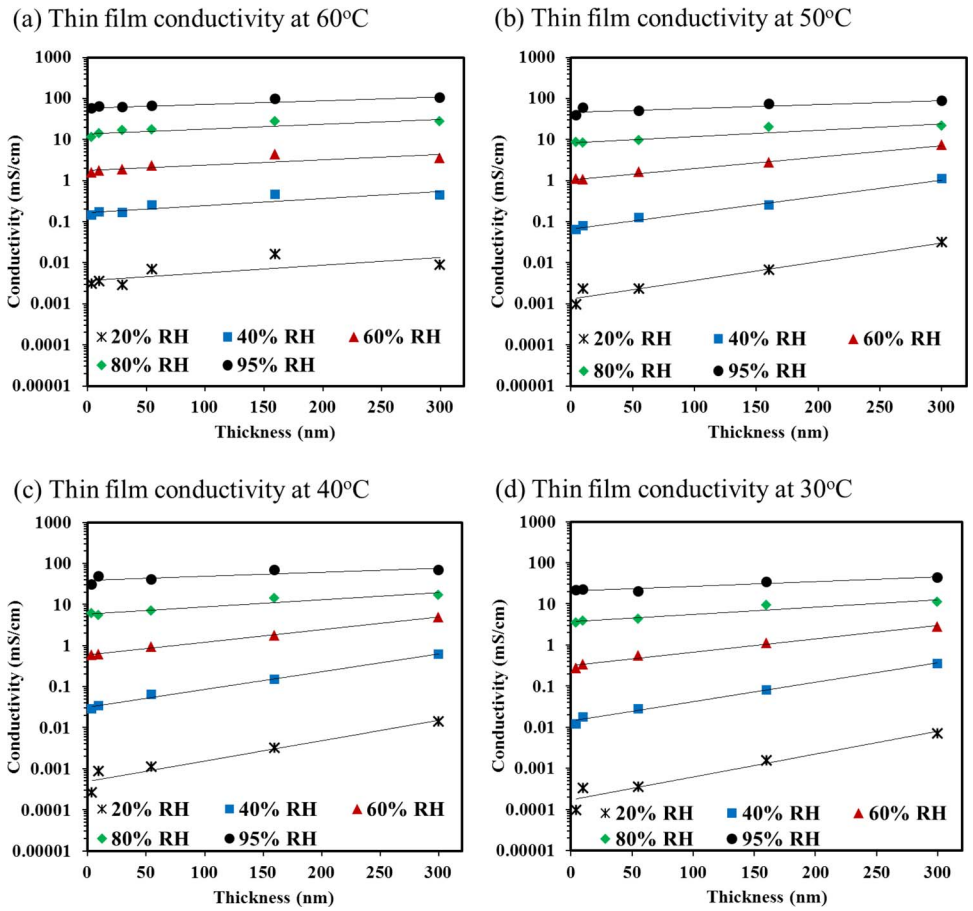

Figure 4. Proton conductivity of the Nafion thin films as a function of film thickness at various relative humidity ranging from 20 to 96% RH at 60°C.

Previously, two distinct behaviors for the thin film surface wettability were reported wherein the surface of the sub-55 nm films were found to be hydrophilic whereas films with thickness above 55 nm were hydrophobic.[35] Interestingly, the bulk conduction property of the film directly correlates with the surface properties. It indicates that free surface of the sub-55 nm films, at least in the unannealed (without any heat-treatment) state, have similar nano-orientation and likely similar intrinsic bulk transport property.

Proton conductivity at higher temperature.—Proton conductivities of the Nafion thin films at different relative humidity and 30–60°C have been presented as a function of thickness in the Figure 4. The equilibration of film at 60°C was ensured according the pre-treatment Protocol-2. First, the measurements were carried out at 60°C, then at lower temperatures in the sequence of 50, 40 and 30°C. It was found that proton conductivity of even the sub-55 nm thin films are thickness-dependent which is contrary to the room temperature measurement. As expected, the proton conductivity decreased with decreasing temperature (Figure 4). Similar thickness-dependency in Nafion thin film proton conductivity was reported by Siroma et al.[21]

At low RH, a clear dependency of proton conductivity on thickness was observed with increase in conductivity noted for increasing thickness. In particular, the conductivity difference between the lowest (4 nm) and the highest (300 nm) thickness films is a factor of two at 60°C as opposed to two orders of magnitude for that at 25°C. On the other hand, at 95% RH, the proton conductivity for the 300 nm film is ∼100 mS/cm which is almost double that of the 4 nm film (∼55 mS/cm). It is noted that the thin films have lower proton conductivity compare to its Nafion 117 membrane that was measured as 135 mS/cm[41] at 50°C and 140 mS/cm[42] at 65°C and both at 100% RH. However, unlike room temperature measurements, the proton conductivity variation between ultra-thin and thicker films at higher temperature is not significant at high RH. Therefore, it is evident that thermal treatment has a significant influence on the observed proton conductivity that might be attributed to two possible reasons – (i) film/substrate interfacial or un-equilibrated excess water (ii) internal structure changes upon heating to 60°C. A further insight may be gained by investigating the film conductivity at 25°C without and with (before and after) 60°C temperature treatment.

Effect of heat-treatment on proton conductivity.—Films for which the conductivity was measured at room temperature (25°C) without any prior high-temperature treatment has been termed as un-treated film. On the other hand, films for which conductivity was measured after 60°C treatment (after equilibration and impedance measurement at 60°C) has been termed as treated film. The proton conductivity at 25°C of both treated and un-treated films has been compared in the Figure 5. To deal with both interfacial/excess water and structural change issues, a prior understanding of water behavior in thin film is required. In practice, the excess water may exist as free water but confined to the film/substrate interfacial region or be tightly bound to substrate. This trapped or tightly bound water in the film may take a long time to equilibrate with the external environment especially at low RH and low temperature. The difference in water content before and after heat-treatment is being referred to as interfacial or non-equilibrated excess water. It is assumed that the interfacial water or non-equilibrated excess water in the film might contribute to the significant enhancement of the proton conductivity in the low RH measurement. At high RH, the change might be insignificant as the film reaches the highest saturation point. In contrast, structural rearrangement might have an impact on the overall change in proton conductivity regardless relative humidity. For the 10 nm film, it was observed that the proton conductivity of the treated film had an overall 5% reduction than that of the un-treated film. It indicates that structural

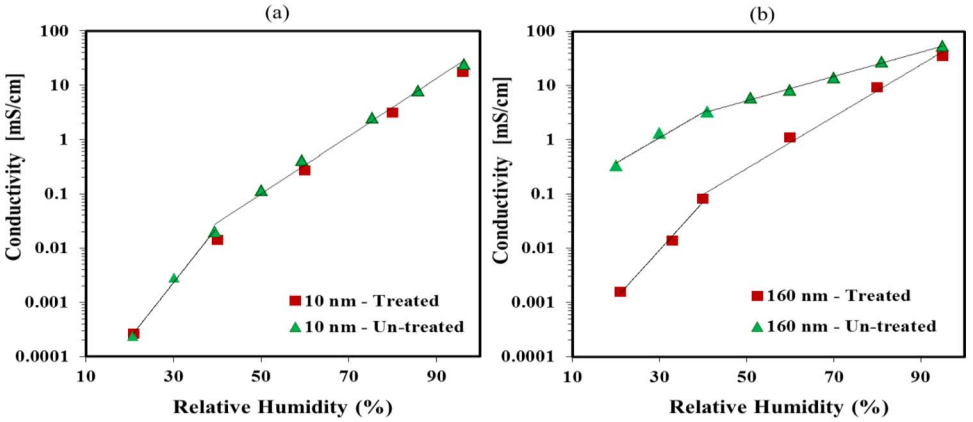

Figure 5. Proton conductivity of thermally treated and un-treated nanofilms at 25°C, for (a) the 10 nm film and (b) the 160 nm film.

rearrangement, if any, has little impact on the proton conductivity. For the 160 nm film, the overall proton conductivity of the treated film was lower than that of the un-treated film where the difference became more significant with decreasing RH. The conductivity of treated film at 95% RH reduced by ~30% compared to that of the un-treated film. However, at low RH, the conductivity reduction upon treatment is few orders of magnitude. The observation suggests that before 60°C treatment, there might have non-equilibrated excess water which attributed higher proton conductivity at low RH. At the same time, equilibration at 60°C may be responsible for the structural rearrangement in such a way that it impedes water uptake. Similar observations in the case of Nafion 117 membrane proton conductivity measurement has been reported.[43] In that study, the membrane conductivity decreased with increasing temperature from 20°C to 45°C due to lose of water at higher temperature and then increased with increasing temperature up to 80°C as water content remain constant after 45°C equilibration. The structural rearrangement and corresponding low proton conductivity for both Nafion thin film and membrane subjected to higher temperature treatment was also reported in many literature.[17,43–47]

It can be summarized that the proton conductivity of ultra-thin film is lower than that of the freestanding membrane regardless of the temperature and relative humidity. The finding of lower proton conductivity in Nafion thin films is consistent with the depressed surface current density and proton conductivity of thin film measured by current sensing AFM[46] and impedance technique[21,26] respectively. The difference becomes more prominent with deceasing RH. A distinct behavior of proton conductivity –the films up to 55 nm have similar but lower than the membrane conductivity, and the thicker films tend to reach membrane like conductivity, at room temperature. The distinct features of bulk proton transport property highly correlate with the two distinct surface wettabilities.[35] In contrast, the conductivity of the films treated at and also measured at 60°C are highly thickness dependent where the conductivity increases with increasing thickness.

Capacitance behavior of the Nafion nanothin films.— The capacitance extracted from EC-2 in terms of three parameters - relative humidity, temperature and film thickness, are discussed. The main goal is to find out whether the capacitance has a dependency on those three parameters and ultimately, to investigate the origin of the capacitance. The capacitance can be calculated by the following formula.[40]

$$C_f = Q_o(\omega_{\max})^{n-1} \quad [3]$$

where, $Q_o = CPE\text{-}T_f$, ω_{max} = the frequency at semicircle maximum, $n = CPE\text{-}P_f$. The capacitances of all the films have been calculated on IDA electrode with 100 μm gap in the inter-digitated electrodes. The calculated capacitances have been normalized by the film thicknesses (F/nm) and have been presented as a function of relative humidity in the Figure 6.

It was found that the film capacitance decreased with increasing relative humidity for all of the thin films ranging 4–300 nm in thickness as shown in Figure 6a. The decreasing capacitance with increasing RH is consistent with the data reported for Nafion 117 membrane.[13] The normalized capacitance also have been plotted as a function of film thickness for different RH in the Figure 6b. A exponential decay of capacitance (F/nm) was observed with increasing thickness. It indicates that the capacitances are highly thickness-dependent.

The capacitance is further dependent on temperature where it was found that the capacitance increased with increasing temperature (see Figure S9 in SI). Moreover, similar exponential decay with increasing thickness was observed for all the temperatures at both low and high relative humidity. The variation of capacitance with relative humidity

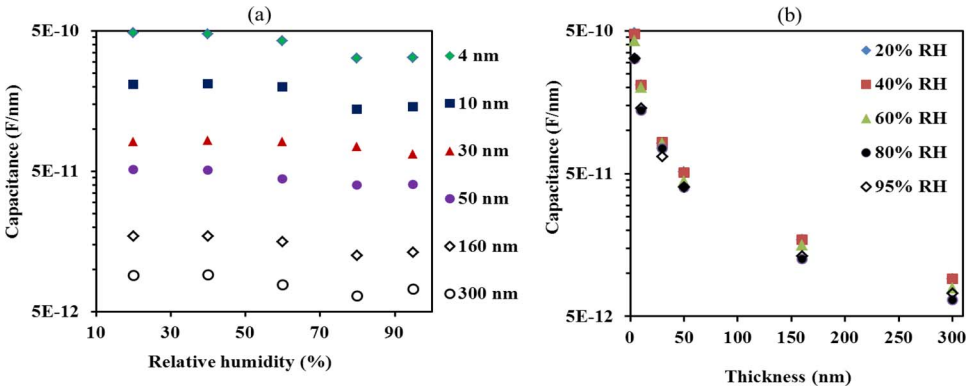

Figure 6. (a) Capacitance of Nafion nanothin films as a function of relative humidity at 60°C for different film thickness. (b) Capacitance of Nafion nanothin films as a function of thickness at 60°C for RH varying from 20% to 95%.

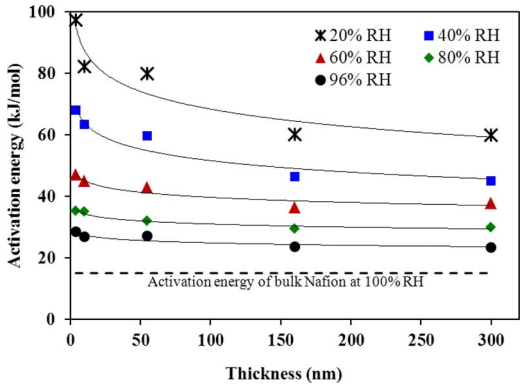

Figure 7. Activation energy of the proton conductivity as a function of film thickness in terms of relative humidity ranging from 20 to 96% RH. Bulk membrane activation energy at 100% RH (dotted line).[21]

and temperature indicates that the capacitance is associated with the film rather than the substrate or the cell. The idea of film capacitance is further supported by the increase of capacitance with an increase in film thickness and film measurment length (electrode spacing). For a homogeneous material, the film capacitance is expected to scale linearly with thickness. Thus, the normalized capacitance remains constant for the same materials. However, the capacitance varied non-linearly with thickness. In fact, the normalized capacitance decayed exponentially rather than stay constant, which may be indicative of the thickness-dependent morphological differences among the thin films that is consistent with grazing incidence small angle X-ray scattering data on our films[37] as well as wettability differences between the sub-55 nm film and thickner films.[35] Measurements were carried out for films on IDA with varying inter-electrode gap (from 30 μm to 500 μm) and number of teeths (see SI Figure S11). The capacitance of film contained between each set pair of electrode, obtained by dividing the total film capacitance with the number of teeth, was found to vary linearly with the inter-electrode gap length. This would be consistent with the film capacitance being proportional to the volume of material contained between the two electrodes. Thus, thickness-dependent capacitance would imply thickness-dependent differences in the internal structure.

Activation energy of the proton conduction in Nafion nanothin films.— It is evident that the proton conductivity is dependent on film treatment protocol. Therefore, extra care was taken for the temperature dependent measurement to extract activation energy. In this regard, all the impedance data was collected at a fixed RH at different temperatures ranging from 60°C to 30°C in the backward direction to avoid any non-equilibrated extra water influence or the effect of structural rearrangement in the conductivity.

Activation energy was calculated using Arrhenius plot and equation 4. Arrhenius plots of conductivity (logarithm of conductivity vs 1/T) for the 4–300 nm films at different RH are shown in SI (Figure S10). As can be noted, each plot was fitted by Arrhenius equation with excellent linearity. The slope of these plots yields the activation energy (E_a) of the proton conductivity (σ) following the following relation between temperature and conductivity:

$$\ln \sigma = \ln \sigma^o - \frac{E_a}{R}.\frac{1}{T} \qquad [4]$$

The activation energy of the thin Nafion films over 20–96% RH range has been plotted as a function of film thickness in Figure 7. The dotted line indicates the activation energy of the bulk membrane - Nafion 117 at the 100% RH. It was found that activation energy of Nafion thin film is thickness-dependent where it decreases logarithmically with increasing thickness. The difference in the activation energies among the thin films varies with the variation of RH. At low RH, the activation energy of the ultra-thin films (4 to 55 nm) was ~30–35% higher than that of the thicker films (160 and 300 nm). In contrast, the activation energy difference at high RH became less significant where 10 to 15% higher activation energy was observed in the ultra-thin films than that of the thicker films. Another vital finding is the higher activation energy in the thin films regardless of thickness compared to that of the bulk membrane. The activation energy of Nafion 117 equilibrated with liquid water was reported to vary from 9 to 14 kJ/mol.[27,28] The activation energy for proton conduction in membranes does not depend on film thickness as observed from the similarity of activation energy for Nafion-112, 117, and 120.[21,27,28] In comparison to membrane form of Nafion, the activation energy of the thin films is 2 to 3 times higher at 40% RH and further increased with decreasing RH. On the other hand, the activation energy of the thin films is closer to the membrane at 96% RH.

The differences in the activation energy of the Nafion membrane and thin films may be attributed to the differences in the internal structural features of Nafion thin films, which can affect either the local proton mobility or the long range transport. As discussed in the literature, the proton conduction in Nafion membrane occurs through 4–6 nm diameter of the nano-channels.[8] It is not clear whether such nano-channels exists in the ultra-thin Nafion films, especially, in the 4 and 10 nm films,[35] and it is plausible that the proton conduction may be impeded due to lack of such well-defined channels in thin films. Also, the substrate may influence the orientation of the molecule to form a lamellar arrangement in these thin films.[14,15,35] Thickness-dependent activation energy would be consistent with the gradual change of structure of the film, perhaps from a lamellar structure of the 4 and 10 nm films to the membrane-like structure of the 300 nm film.[35] It is not directly evident which conduction mechanism is dominating, however, high activation energy in the thin film indicates that slower mechanistic pathway i.e., surface conduction mechanism[29] is dominating over the Grotthuss (hopping) mechanism and vehicular/en-mass diffusion mechanism.[30–32]

Conclusions

A Measurement protocol has been reported for impedance of Nafion nanothin films on the IDA of Au electrode system including impedance response, equivalent circuit design, data fitting and analyses. The proton conductivity and the capacitance of the Nafion thin film has been discussed with respect to the treatment condition, relative humidity, temperature, thickness and IDA geometry. It was found that the proton conductivity of the Nafion nanothin films is lower than that of the membrane regardless of the temperature, the relative humidity and the film thickness. Film thickness and treatment protocols plus thermal history are the two influencing parameters on the proton conductivity of the Nafion nanothin films. For room temperature measurements (25°C, Protocol-1), the proton conductivity of sub-55 nm Nafion thin films was found to be independent of thickness whereas that of the thicker films was thickness-dependent, approaching that of the membrane. The two distinct behaviors of the proton conductivity are highly consistent with the distinct surface wettability of the thin film. In contrast, measurements at high temperature (60°C, protocol-2), indicated that the conductivity of all thin Nafion films is thickness-dependent, with decreasing conductivity for decreasing thickness. Similarly, activation energy was also thickness dependent but in contrast, increases logarithmically with decreasing thickness. Thickness-dependent higher activation energy compared to that of the membrane directly correlate with low proton conductivity of the thin films. Low proton conductivity of thin films is consistent with several other literature evidences.[21,26,46]

Acknowledgment

The financial assistance for this work was provided by the Natural Sciences and Engineering Research Council of Canada (NSERC) and the Early Researcher Award (for Kunal Karan), Ontario Ministry

of Research. The authors acknowledge Bryan Szeto at the National Institute for Nanotechnology for fabrication of the IDE arrays.

References

1. S. Holdcroft, *Chem. Mater.*, **26**, 381 (2014).
2. S. A. Grigoriev, V. I. Porembsky, and V. N. Fateev, *J. Hydrogen Energy*, **31**, 171 (2006).
3. R. Brimblecombe, A. Koo, G. C. Dismukes, G. F. Swiegers, and L. Spiccia, *J. Am. Chem. Soc.*, **132**, 2892 (2010).
4. R. K. Hocking, R. Brimblecombe, L.-Y. Chang, A. Singh, M. H. Cheah, C. Glover, W. H. Casey, and L. Spiccia, *Nat. Chem.*, **3**, 461 (2011).
5. W. Kim, T. Seok, and W. Choi, *Energy Environ. Sci.*, **5**, 6066 (2012).
6. K. More, R. Borup, and K. Reeves, *ECS Trans.*, **3**, 717 (2006).
7. W. Y. Hsu and T. D. Gierke, *Macromolecules*, **15**, 101 (1982).
8. K. Schmidt-Roh and Q. Chen, *Nat. Mater*, **7**, 75 (2008).
9. F. T. Wagner, B. Lakshmanan, and M. F. Mathias, *J. Phy. Chem. Lett.*, **1**(14), 2204 (2010).
10. T. Soboleva, Z. Xie, Z. Shi, E. Tsang, T. Navessin, and S. Holdcroft, *J. Electroanal. Chem., J. Electroanal. Chem.*, **622**, 145 (2008).
11. J. Halim, F. N. Buchi, O. Haas, M. Stamm, and G. G. Scherer, *Electrochim. Acta, Electrochim. Acta*, **39**, 1303 (1994).
12. S. Slade, S. A. Campbell, T. R. Ralph, and F. C. Walsh, *J. Electrochem. Soc., J. Electrochem. Soc.* **149**(12), 1556 (2002).
13. R. Yadav and P. S. Fedkiw, *J. Electrochem. Soc., J. Electrochem. Soc.*, **159**(3), 340 (2012).
14. A. J. Dura, S. V. Murthi, M. Hartman, K. S. Satija, and F. C. Majkrzak, *Macromolecules*, **42**, 4769 (2009).
15. L. D. Wood, J. Chlistunoff, J. Majewski, and L. R. Borup, *J. Am. Chem. Soc.*, **131**, 18096 (2009).
16. M. Bass, A. Berman, A. Singh, O. Konovalov, and V. Freger, *Macromolecules*, **44**, 2893 (2011).
17. M. A. Modestino, A. Kusoglu, A. Hexemer, A. Z. Weber, and R. A. Segalman, *Macromolecules*, **45**, 4681 (2012).
18. A. Kongkanand, *J. Phys. Chem. C*, **115**, 11318 (2011).
19. K. S. Dishari and M. A. Hickner, *ACS Macro Lett.*, **1**, 291 (2012).
20. D. K. Paul, A. Fraser, and K. Karan, *Electrochem. Comm.*, **13**(8), 774 (2011).
21. Z. Siroma, R. Kakitsubo, N. Fujiwara, T. Ioroi, S-I. Yamazaki, and K. Yasuda, *J. of Power Sources*, **189**, 994 (2009).
22. S. A. Eastman, S. Kim, K. A. Page, B. W. Rowe, S. Kang, and C. L. Soles, *Macromolecules*, **45**, 7920 (2012).
23. G. C. Abuin, C. M. Fuertes, and H. R. Corti, *J. of Membrane Sci.*, **428**, 507 (2013).
24. K. A. Page, A. Kusoglu, C. M. Stafford, S. Kim, R. J. Kline, and A. Z. Weber, *Nano Letters*, **14**(5), 2299 (2014).
25. A. Kusoglu, D. Kushner, D. K. Paul, K. Karan, M. A. Hickner, and A. Z. Weber, *Adv. Funct. Mater.*
26. Y. Nagao, *J. Phys. Chem. C*, **117**, 3294 (2013).
27. T. A. Zawodzinski, S. Gottesfeld, S. Shoichet, and T. J. McCarthy, *J. Appl. Electrochem.*, **23**, 86 (1993).
28. P. Dimitrova, K. A. Friedrich, B. Vogt, and U. J. Stimming, *Electroanal. Chem.*, **532**, 75 (2002).
29. P. Choi, N. H. Jalani, and R. Datta, *J. Electrochem. Soc.*, **152**(3), E123 (2005).
30. M. Eikerling, A. A. Kornyshev, A. Kuznetsov, M. J. Ulstrup, and S. Walbran, *J. Phys. Chem. B*, **105**, 3646 (2001).
31. S. J. Paddison and R. Paul, *Phys. Chem. Chem. Phys.*, **4**, 1158 (2002).
32. K. D. Kreuer, S. J. Paddison, E. Spohr, and M. Schuster, *Chem. Rev.*, **104**, 4637 (2004).
33. M. Eigen, *Angew. Chem.*, **75**, 489 (1963).
34. G. Zundel and H. Z. Metzger, *Naturforsch.*, **22a**, 1412 (1967).
35. D. K. Paul, K. Karan, J. Giorgi, A. Docoslis, and J. Pearce, *Macromolecules*, **46**(9), 3461 (2013).
36. D. K. Paul, A. Fraser, J. Pearce, and K. Karan, *ECS Trans.*, **41**, 1393 (2011).
37. M. A. Modestino, D. K. Paul, S. Dishari, S. A. Petrina, F. I. Allen, M. A. Hickner, K. Karan, R. A. Segalman, and A. Z. Weber, *Macromolecules*, **46**(3), 867 (2013).
38. S. D. Mikhailenko, M. D. Guiver, and S. Kaliaguine, *Solid State Ionics*, **179**, 619 (2008).
39. C. H. Lee, H. B. Park, Y. M. Lee, and R. D. Lee, *Industrial & Engineering Chemistry Research*, **44**(20), 7617 (2005).
40. P. Andrew and S. S. Leis, *Appl Environ Microbiol.*, **11**(8), 4801 (2005).
41. K. J. Miura, O. Hong, K. Yashiro, Y. Nigara, T. Kawada, and J. Mizusaki, *Transaction of Material Research Society, Japan*, **26**, 1079 (2001).
42. K. M. Nouel and P. S. Fedkiw, *Electrochim. Acta*, **43**, 2381 (1998).
43. Y. Sone, P. Ekdunge, and D. Simsonsson, *J. Electrochem. Soc.*, **143**, 1254 (1996).
44. D. K. Paul and K. Karan, *J. Phy. Chem. C*, **118**, 1828 (2014).
45. J. Benziger, A. Bocarsly, M. J. Cheah, P. Majsztrik, B. Satterfield, and Q. Zhao, *Fuel Cells and Hydrogen Storage Structure and Bonding*, **141**, 85 (2011).
46. A. Ohira, S. Kuroda, H. F. M. Mohamed, and B. Tavernier, *Phys. Chem. Chem. Phys.*, **15**, 11494 (2013).
47. D. K. Paul and K. Karan, *ECS Trans.*, **50**(2), 951 (2013).
48. C. S. Hsu and F. Mansfeld, *Corrosion*, **57**, 747 (2001).